Title

CRY1-CBS binding regulates circadian clock function and metabolism

Journal

The FEBS Journal, 288(2)

ISSN

1742-464X

Authors

Cal-Kayitmazbatir, Sibel
Kulkoyluoglu-Cotul, Eylem
Growe, Jacqueline
et al.

Publication Date

2021

DOI

10.1111/febs.15360

Peer reviewed

The human CRY1 tail controls circadian timing by regulating its association with CLOCK:BMAL1

Gian Carlo G. Parico[a], Ivette Perez[a], Jennifer L. Fribourgh[a], Britney N. Hernandez[a], Hsiau-Wei Lee[a], and Carrie L. Partch[a,b,1]

[a]Department of Chemistry and Biochemistry, University of California, Santa Cruz, CA 95064; and [b]Center for Circadian Biology, University of California San Diego, La Jolla, CA 92093

Edited by Joseph S. Takahashi, The University of Texas Southwestern Medical Center, Dallas, TX, and approved September 29, 2020 (received for review November 22, 2019)

Circadian rhythms are generated by interlocked transcription–translation feedback loops that establish cell-autonomous biological timing of ∼24 h. Mutations in core clock genes that alter their stability or affinity for one another lead to changes in circadian period. The human CRY1Δ11 mutant lengthens circadian period to cause delayed sleep phase disorder (DSPD), characterized by a very late onset of sleep. CRY1 is a repressor that binds to the transcription factor CLOCK:BMAL1 to inhibit its activity and close the core feedback loop. We previously showed how the PHR (photolyase homology region) domain of CRY1 interacts with distinct sites on CLOCK and BMAL1 to sequester the transactivation domain from coactivators. However, the Δ11 variant alters an intrinsically disordered tail in CRY1 downstream of the PHR. We show here that the CRY1 tail, and in particular the region encoded by exon 11, modulates the affinity of the PHR domain for CLOCK:BMAL1. The PHR-binding epitope in exon 11 is necessary and sufficient to disrupt the interaction between CRY1 and the subunit CLOCK. Moreover, PHR–tail interactions are conserved in the paralog CRY2 and reduced when either CRY is bound to the circadian corepressor PERIOD2. Discovery of this autoregulatory role for the mammalian CRY1 tail and conservation of PHR–tail interactions in both mammalian cryptochromes highlights functional conservation with plant and insect cryptochromes, which also utilize PHR–tail interactions to reversibly control their activity.

circadian rhythms | cryptochrome | intrinsically disordered protein | CON NMR | delayed sleep phase disorder

Circadian rhythms coordinate behavior and physiology with the 24-h solar day. At the molecular level, over 40% of the genome is temporally regulated in a circadian manner (1). In the core transcription/translation feedback loop of the clock, the heterodimeric transcription factor CLOCK:BMAL1 (CLOCK [circadian locomotor cycles output kaput]; BMAL1 [brain and muscle ARNT-like protein 1]) promotes transcription of its own repressors, period (PER1/2) and cryptochrome (CRY1/2) (2). Cryptochromes facilitate the direct interaction of PER–CRY repressive complexes with CLOCK:BMAL1 (3) and sequester the transactivation domain (TAD) of BMAL1 from coactivators to directly inhibit its activity (4). We previously showed that changing the affinity of CRY1 for the BMAL1 TAD can alter circadian timing (4, 5), presumably by shortening or lengthening the duration of repression in the feedback loop. Similarly, missense mutations within other core clock genes that alter their stability or activity can change the circadian period (6–12). Variants that shorten circadian period correlate with the earlier sleep/wake times associated with advanced sleep phase disorder (ASPD), while delayed sleep phase disorder (DSPD) is characterized by a longer than normal circadian period (>24.2 h) and later than normal sleep/wake times (13).

One form of familial DSPD arises from a variant of CRY1 (CRY1Δ11) that is as prevalent as 1 in 75 in certain populations (14). CRY1Δ11 disrupts a splice site leading to the in-frame deletion of exon 11, thus removing 24 residues within the disordered C-terminal tail of CRY1. While only the PHR domain of CRY1 is necessary to reconstitute circadian rhythms in $Cry1^{-/-};Cry2^{-/-};Per2^{Luc}$ cells (15), the tails can modulate the period and/or amplitude of cycling, as evidenced by reconstitution assays using chimeras swapping the CRY1 and CRY2 tails (15–17) or assessing posttranslational modifications like phosphorylation in the tail (18–20). Mechanistically, the CRY1 PHR binds directly to both CLOCK (3, 21) and BMAL1 (4, 5, 22) subunits as well as the CRY-binding domain (CBD) of PER2 (23) to form the central linchpin of vertebrate circadian repressive complexes (24). This suggests that the CRY1Δ11 variant, which enhances both the coimmunoprecipitation with CLOCK:BMAL1 and the transcriptional repressive state in cells (14), may alleviate an interaction between the CRY1 tail and PHR domain to increase its affinity for CLOCK:BMAL1.

Here, we identify an autoinhibitory role for exon 11 of the CRY1 tail in regulating its association with CLOCK:BMAL1, and therefore, control of the molecular circadian clock. We show that the CRY1 C-terminal tail interacts directly with its PHR domain; using biochemical analyses and solution NMR spectroscopy, we discovered that exon 11 comprises one of two linear epitopes in the tail that bind to the PHR. Exon 11 is necessary and sufficient to compete with the PAS-B domain of CLOCK for binding to CRY1. Consistent with this, full-length CRY1 has decreased affinity for the PAS domain core of CLOCK:BMAL1

Significance

Cryptochromes (CRYs) are structurally defined by an evolutionarily conserved PHR domain and divergent intrinsically disordered tails of variable length. Photosensory cryptochromes from plants and insects use reversible interactions between their PHR domain and disordered tails to control signal transduction. Although several studies have suggested that the tails of vertebrate cryptochromes influence circadian rhythms, nothing was known about the molecular mechanism. We used the DSPD CRY1Δ11 splice site variant to discover that the CRY1 tail interacts directly with its PHR domain and that the segment encoded by exon 11 regulates its affinity for CLOCK:BMAL1. Developing mechanistic insight into CRY1 regulation reveals common signaling mechanisms in cryptochromes and suggests strategies for treating prevalent circadian rhythm and sleep disorders.

Author contributions: G.C.G.P., H.-W.L., and C.L.P. designed research; G.C.G.P., I.P., J.L.F., B.N.H., and H.-W.L. performed research; G.C.G.P., I.P., J.L.F., and B.N.H. contributed new reagents/analytic tools; G.C.G.P., I.P., J.L.F., and H.-W.L. analyzed data; G.C.G.P. and C.L.P. wrote the paper; and C.L.P. supervised project and secured funding.

The authors declare no competing interest.

This article is a PNAS Direct Submission.

[1]To whom correspondence may be addressed. Email: cpartch@ucsc.edu.

This article contains supporting information online at https://www.pnas.org/lookup/suppl/doi:10.1073/pnas.1920653117/-/DCSupplemental.

First published October 26, 2020.

compared to CRY1Δ11 or the isolated PHR domain. Notably, PHR–tail interactions are conserved in the paralog CRY2 and formation of a stable complex between the CBD of PER2 and the PHR domain of CRY1 or CRY2 interferes with PHR–tail interactions. These data point toward a conserved role for cryptochrome C-terminal tails as regulators of CRY function via direct interaction with the PHR domain.

Results

The CRY1 Tail Binds Directly to the CRY1 PHR. We used fluorescence polarization (FP) assays to explore binding of a fluorescently labeled human CRY1 tail to the PHR domain *in trans* (Fig. 1*A*). The resulting binding curve is consistent with single-site protein-ligand binding and fits to an equilibrium dissociation constant (K_D) of about 5 μM (Fig. 1 *B* and *C*). The Δ11 version of the hCRY1 tail interacts with about fourfold lower affinity, demonstrating that exon 11 plays an important role in binding the PHR domain (Fig. 1 *B* and *C*). A peptide encoding the isolated exon 11 also binds to the PHR domain, but with lower affinity similar to that of the Δ11 tail, suggesting that additional sites on the CRY1 tail contribute to PHR binding.

Using an exon-based truncation analysis of the tail, we determined that exons 10 and 11 comprise the minimal binding region of the hCRY1 tail for the PHR domain (Fig. 1 *B* and *C*). The mouse CRY1 tail, which contains a short repeat insertion within exon 10, binds to its PHR with a similar affinity to the human tail (*SI Appendix*, Fig. S1). Finally, our data suggest that exon 12 does not enhance affinity for the PHR domain (Fig. 1 *B* and *C*). This was surprising since posttranslational modification within the region encoded by exon 12 apparently regulates the interaction of CRY1 with its E3 ubiquitin ligase to influence circadian rhythms (19, 20). Phosphorylation of S588 in exon 12 of mouse CRY1 (S568 in humans) after DNA damage increases its stability, as does the corresponding phosphomimetic mutation S588D (18–20). Consistent with our observation that exon 12 does not appear to contribute to PHR binding, we found no change in affinity of the S588D CRY1 tail for the PHR domain (*SI Appendix*, Fig. S1 *C* and *D*).

NMR Spectroscopy Maps PHR-Binding Epitopes in the CRY1 Tail. To further map the PHR-binding epitopes on the tail, we used NMR spectroscopy. Backbone-based ^{1}H–^{15}N heteronuclear single-quantum coherence (HSQC) experiments probe the chemical environment of all nonproline residues as individual peaks; however, these spectra exhibit severe peak overlap in the case of long intrinsically disordered proteins (IDPs) such as the CRY1 tail (Fig. 2*A*) (25, 26). To circumvent this problem, we turned to ^{13}C carbon-detected methods such as the ^{13}C–^{15}N CON to increase peak dispersion, and therefore our resolution, on this IDP (27). The CON spectrum of the CRY1 tail exhibited excellent peak dispersion that allowed us to visualize and unambiguously assign 81% of the backbone chemical shifts (Fig. 2*B*).

To probe the role of exon 11 in the CRY1 tail/PHR interaction, we added unlabeled CRY1 PHR domain to the ^{13}C,^{15}N-labeled CRY1 tail and monitored chemical shift perturbations in the tail. We were limited to some degree by the solubility and stability of the CRY1 PHR domain under our NMR conditions, but under equimolar concentrations of tail and PHR, we identified a number of peaks that exhibited PHR-dependent changes indicative of binding (Fig. 2 *B* and *C*). Another advantage of carbon-detected methods is their ability to visualize proline chemical shifts, often enriched in IDPs, that cannot be detected using standard ^{1}H–^{15}N HSQC spectra (Fig. 2 *C* and *D*). For the most part, we observed broadening at select peaks within the ^{13}C,^{15}N-labeled CRY1 tail upon binding to the PHR, likely due to the large size of the PHR domain (~55 kDa) (Fig. 2 *B*, *C*, and *E*). However, some clusters of peaks in exons 10 and 11 demonstrated changes in chemical shift (Fig. 2*F*), including a hydrophobic patch in exon 10 that is composed of the motif Phe–Met–Gly–Tyr and several histidines in exon 11 that are conserved (Fig. 2 *G*–*K*, and *SI Appendix*, Fig. S2). These same peaks are also broadened relative to the rest of the

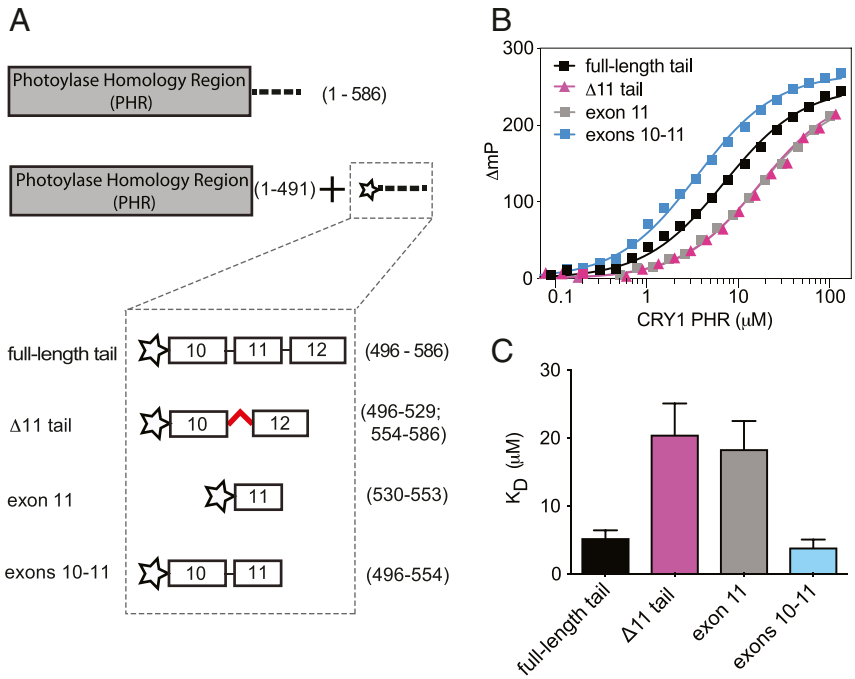

Fig. 1. Exons 10 and 11 in the CRY1 tail are required for PHR binding. (*A*) Domain architecture of full-length human CRY1 and the constructs used in FP experiments, comprising the PHR (residues 1 to 491, gray box) and tail (residues 492 to 586, dashed line) with various truncations; the N-terminal fluorescein (FAM) label is depicted as a star. (*B*) FP binding curves of fluorescently labeled human tail constructs to the CRY1 PHR. Plot shows the mean representative binding curves of duplicate samples ± SD (of $n = 3$ independent assays). Curve represents fit to one-site binding (Prism). (*C*) Affinities of FAM–tail constructs for the PHR derived from FP binding assays ($n = 3$ independent assays ± SD).

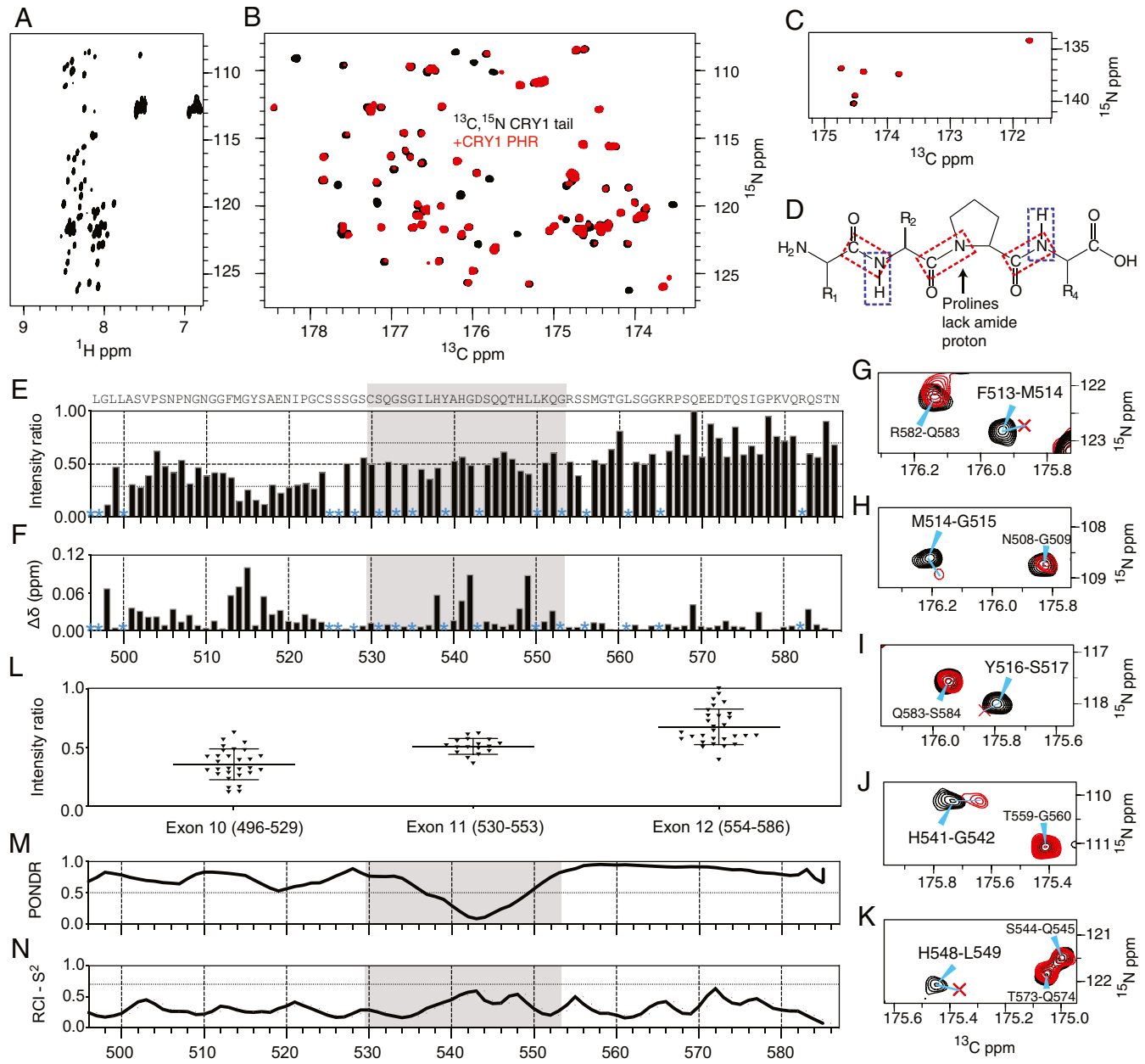

Fig. 2. NMR spectroscopy maps the PHR binding site on the CRY1 tail. (*A*) ^{1}H–^{15}N HSQC spectrum of the isolated ^{15}N-labeled CRY1 tail at 120 μM. (*B*) ^{13}C–^{15}N CON spectra of the ^{13}C,^{15}N-labeled CRY1 tail at 120 μM alone (black) or in the presence of 120 μM CRY1 PHR (red) (*C*), proline-specific region of the ^{13}C–^{15}N CON spectrum of the ^{13}C,^{15}N-labeled CRY1 tail ± CRY1 PHR (as in *B*). (*D*) Schematic of proline-containing peptide backbone, highlighting the correlations visualized by ^{1}H–^{15}N HSQC (blue box) or ^{13}C–^{15}N CON (red box). (*E* and *F*) Relative intensity (*E*) and chemical shift perturbation (Δδ) (*F*) of the ^{13}C,^{15}N-labeled CRY1 tail upon addition of equimolar CRY1 PHR. Asterisk, unassigned or overlapping peaks excluded from the analysis. Exon 11 is represented by a gray box. In *E*, dashed horizontal line represents the mean intensity ratio ($I_{tail+PHR}/I_{tail\ alone}$), while the dotted lines represent SEM. Peaks are referred to by the number of the nitrogen of the ^{13}C–^{15}N peptide bond. (*G*–*K*) Zoom-in on ^{13}C–^{15}N CON spectra peaks (^{13}C carbonyl of F513, M514, Y516, H541, and H548, respectively) that are severely broadened or perturbed upon addition of CRY1 PHR. Residues along a C–N bond point to their corresponding peaks with a cyan arrow, and severely broadened peaks with intensities below the base contour level are labeled with a red "x." (*L*) NMR intensity ratios ($I_{tail+PHR}/I_{tail\ alone}$) grouped by exon (mean ratio per exon ± SD). (*M*) PONDR prediction of a disorder in the CRY1 tail with an ordered minimum in exon 11. (*N*) Random coil index (RCI) predicts lack of secondary structure (model-free parameter $S^2 < 0.7$) from NMR chemical shift assignments.

tail, suggesting that these residues are hotspots for interacting with the PHR (Fig. 2*E*). An exon-based analysis of peak broadening demonstrates that it occurs to the highest extent in exons 10 to 11, and to a lesser degree in exon 12 (Fig. 2*L*), corroborating our FP data that the minimal binding region on the tail for interacting with the PHR domain lies within exons 10 to 11.

We also utilized the NMR data to probe structural characteristics of the isolated CRY1 tail. The narrow proton chemical shift dispersion and overlap of peaks in the ^{1}H–^{15}N HSQC spectrum is representative of a typical IDP (Fig. 2*A*), in agreement with circular dichroism data of the CRY1 tail (28). Although the computational algorithm PONDR predicts that the CRY1 tail is highly disordered, it suggested that there may be some propensity for structure within an ordered "minimum" centered around the sequence encoded by exon 11 (Fig. 2*M*) (29); these local, ordered minima have been implicated as linear

binding epitopes within other IDPs (30). However, a quantitative comparison of CRY1 tail NMR data to the chemical shift index (31) revealed that the entire tail lacks secondary structure in the absence of the PHR domain (Fig. 2*N*). Further studies could identify whether any regions in the tail, such as exon 11, might adopt secondary structure upon binding to the PHR domain.

Exon 11 Is Necessary and Sufficient to Regulate the Interaction between CRY1 and CLOCK. Given that exon 11 plays an important role in the interaction between the CRY1 tail and its PHR domain, we next wanted to determine how it could regulate binding between the CRY1 PHR and CLOCK:BMAL1. There are two distinct interfaces for interaction with the CLOCK:-BMAL1 heterodimer on the CRY1 PHR: the coiled-coil (CC) helix of CRY1 binds to the transactivation domain (TAD) of BMAL1 (4, 28), while the secondary pocket of CRY1 binds directly to CLOCK PAS-B (Fig. 3*A*) (3, 21). We established FP-based binding assays for the PHR domain using fluorescently labeled BMAL1 TAD (4) or CLOCK PAS-B (*SI Appendix*, Fig. S3 *A–F*), allowing us to form complexes of the PHR with either target and determine the ability of exogenous tail to compete for interaction on the PHR domain *in trans*. Titrating CRY1 tail into a CRY1 PHR:BMAL1 TAD complex did not result in any changes in FP, demonstrating that the CRY1 tail does not play a role in regulating the interaction between the CRY1 PHR and the BMAL1 TAD (Fig. 3*B*). However, titrating the CRY1 tail to a CRY1 PHR:CLOCK PAS-B complex caused a dose-dependent decrease in FP signal to levels observed with the isolated CLOCK PAS-B, demonstrating that the tail could displace CLOCK PAS-B from the CRY1 PHR domain (Fig. 3*C*).

To determine a role for exon 11 in displacement of CLOCK PAS-B from the CRY1 PHR, we asked whether a peptide comprising the isolated exon 11 could also displace CLOCK PAS-B from the CRY1 PHR. As shown in Fig. 3*C*, exon 11 also competed CLOCK PAS-B from the PHR domain, albeit with a modest reduction in efficiency relative to the full-length tail (tail IC_{50} = 0.72 ± 0.66 μM; exon 11 IC_{50} = 1.43 ± 1.06 μM). By contrast, the Δ11 tail had no effect on the CRY1 PHR:CLOCK PAS-B complex (Fig. 3*C*). Therefore, exon 11 is necessary and sufficient to regulate the interaction between CLOCK PAS-B and the CRY1 PHR domain. Exon 11 shares sequence attributes with other intrinsically disordered inhibitory modules (idIMs) involved in autoinhibition, which have a mean length of 24 ± 13 residues (exon 11 is 24 residues) and are often modified in splicing isoforms (32). Since the Δ11 tail cannot displace CLOCK PAS-B, it appears that although exon 10 contributes to PHR binding, it does not play a direct role in regulating the interaction between the CRY1 PHR domain and CLOCK PAS-B. This is consistent with data suggesting that residues encoded by exon 10 region bind near the FAD-binding pocket on CRY1, distal from the secondary pocket where CLOCK binds (33).

One prediction of our model is that both CRY1Δ11 and the tailless CRY1 PHR domain should have higher affinity for the PAS domain core of CLOCK:BMAL1 relative to full-length CRY1. We used biolayer interferometry (BLI) to quantitatively assess CRY1 binding to the immobilized PAS domain core comprising the tandem PAS-AB domain heterodimer. Importantly, our previous studies demonstrated that association with CRY1 absolutely depends on CLOCK PAS-B docking into the secondary pocket of CRY1 (3, 21). We tracked the binding kinetics (association and dissociation) of CRY1 over time (Fig. 3 *D* and *E*, and *SI Appendix*, Fig. S3*K*) to confirm that both CRY1Δ11 and the isolated PHR have a higher affinity for the CLOCK:BMAL1 PAS domain core than full-length CRY1 (Fig. 3*F*). Analysis of the kinetic binding data suggested that the decrease in affinity of full-length CRY1 for CLOCK is due to a modest decrease in the association rate (k_{on}) (Fig. 3*G*) rather than an increase in the dissociation rate (k_{off}) (Fig. 3*H*), consistent with other proteins that have autoinhibitory domains (34, 35). Furthermore, the kinetic association rate k_{on} between full-length CRY1 and the PAS domain core of CLOCK:BMAL1 PAS-AB (4.73×10^4 $M^{-1}{\cdot}s^{-1}$) still falls within the typical diffusion-limited regime (10^4 to 10^7 $M^{-1}{\cdot}s^{-1}$), rather than the conformational change-limited regime ($<10^4$ $M^{-1}{\cdot}s^{-1}$), suggesting that formation of the autoinhibitory complex of CRY1 occurs transiently (36). We also measured the equilibrium binding response relative to the concentration of CRY1 titrant (Fig. 3*I*, and *SI Appendix*, Fig. S3*L*) to observe that CRY1Δ11 and the PHR domain both have a higher affinity than full-length CRY1 (Fig. 3*J*). Therefore, both kinetic and steady-state analyses show that CRY1Δ11 and the CRY1 PHR domain have similar affinities for CLOCK, thus emphasizing the essential role of the tail, and exon 11 in particular, as an autoinhibitory module that regulates CRY1 association with CLOCK:BMAL1.

Cells expressing CRY1Δ11 exhibit gene expression profiles consistent with stronger repression of CLOCK:BMAL1 (14). To confirm that the enhanced affinity of CRY1Δ11 for CLOCK directly enhances its ability to repress transcriptional activation by CLOCK:BMAL1, we performed *Per1-luc* luciferase reporter assays in HEK293T cells (Fig. 3*K*). CRY1 is already a potent repressor of CLOCK:BMAL1 and its multivalent interactions with CLOCK and BMAL1 subunits can partially compensate for changes in affinity at only one of the binding sites (4, 21, 37); therefore, we used a series of *Clock* or *Bmal1* mutants that reduce affinity between CRY1 and CLOCK:BMAL1 at either the PAS domain core (*Clock* W362A) or the BMAL1 TAD (*Bmal1* L606A/L607A or the 619X truncation), reasoning that stronger binding by CRY1Δ11 would rescue repression. Indeed, expression of CRY1Δ11 consistently led to significantly increased repression, not only with wild-type CLOCK:BMAL1, but also with CLOCK and BMAL1 mutants (Fig. 3*K*), even though CRY1Δ11 was expressed to the same extent as full-length CRY1 (Fig. 3*L*). Therefore, by enhancing CRY1 affinity for CLOCK at the PAS domain core, the Δ11 allele serves as a better repressor of CLOCK:BMAL1.

PER2 Attenuates the CRY1 PHR–Tail Interaction. Chromatin immuno precipitation-sequencing data of native clock proteins in mouse liver throughout the day revealed that CRY1 participates in two temporally distinct repressive complexes on DNA (38): an "early" complex at circadian time 16 (CT16) to CT20, when CRY1 is also found in large, heterogeneous complexes with CRY2, PER proteins and other epigenetic regulators (39), and a "late" complex at CT0 to CT4 where CRY1 is bound to CLOCK:BMAL1 in the absence of other core clock proteins (24, 40, 41). Therefore, CRY1 has a distinct role in the clock, in line with studies showing that it is critical for sustaining cellular circadian rhythms in dissociated SCN neurons (42), and that it can work as a repressor both with PER proteins and independently of them (24, 40, 41).

Crystal structures reveal that the CBD of PER2 wraps around the CRY PHR domain to make contacts near both of the CLOCK and BMAL1 binding sites (Fig. 4*A*) (3, 23, 43). Given that exon 11 can displace CLOCK PAS-B from the CRY1 secondary pocket, we wanted to see whether the PER2 CBD could affect interaction of the tail with the CRY1 PHR domain. First, we examined binding of the fluorescently labeled tail to either CRY1 PHR or a preformed CRY1 PHR:PER2 CBD complex, and found that PER2 decreased tail binding on the PHR domain by at least 10-fold (Fig. 4*B*). By contrast, the presence of the tail in full-length CRY1 did not affect the affinity between CRY1 and the PER2 CBD (Fig. 4*C*). Therefore, even though the tail is tethered and thus present at a higher localized effective concentration, the PER2 CBD binds to CRY with low nanomolar affinity (23) and is able to outcompete the tail for binding to the PHR domain. We further tested this hypothesis by titrating the

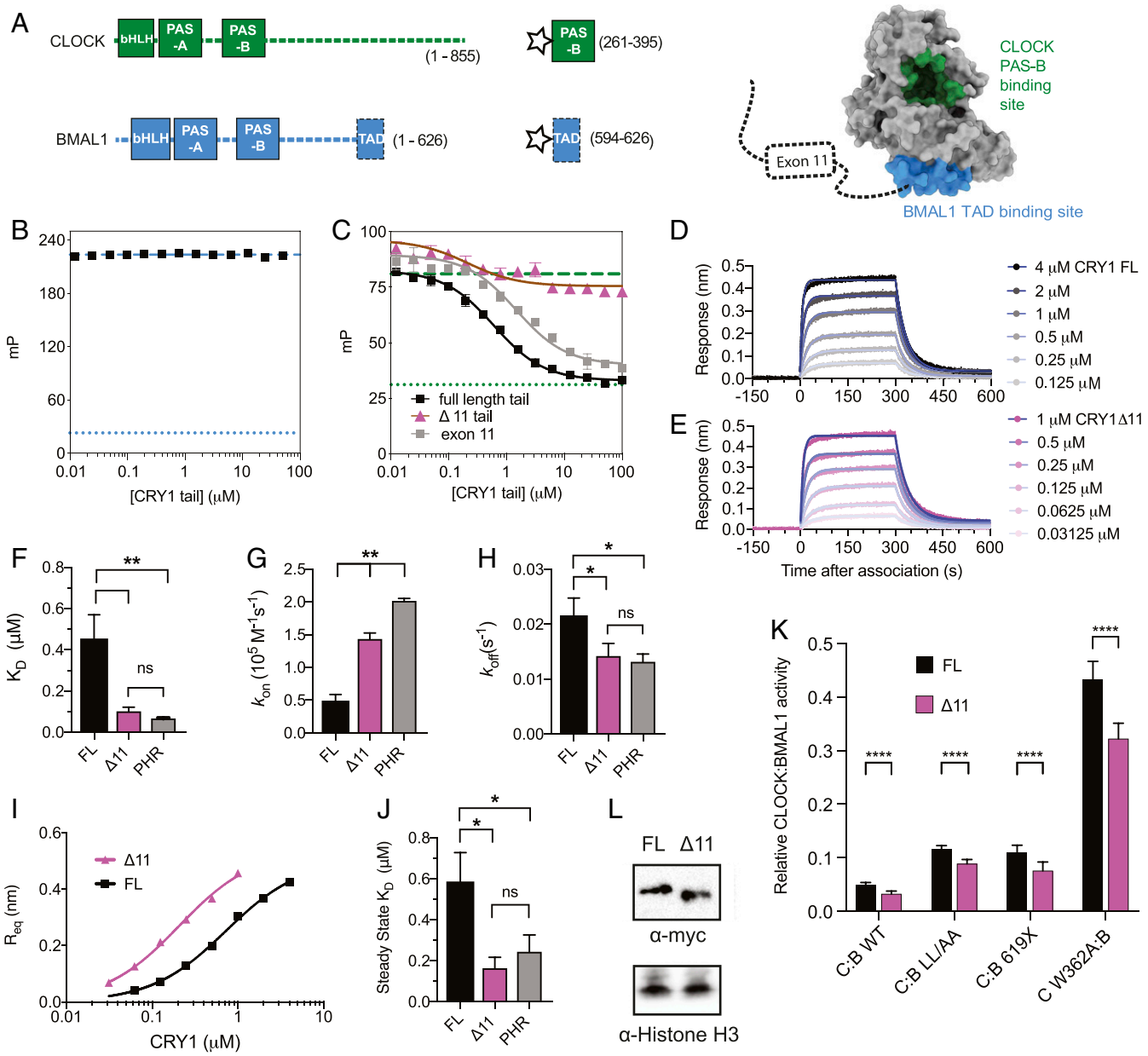

Fig. 3. Exon 11 competes with CLOCK PAS-B to reduce CRY1 affinity for CLOCK:BMAL1. (*A*) Domain architecture of CLOCK and BMAL1. Starred constructs represent those used for FP assays. (*Right*) CLOCK (green) and BMAL1 (blue) binding sites mapped onto the CRY1 PHR (PDB: 5T5X). (*B*) FP-based equilibrium competition assay in which the CRY1 tail (black) is titrated into a mixture of 4 μM CRY1 PHR and 20 nM fluorescently labeled BMAL1 TAD probe. Mean FP signal ($n = 13$ points from same plate as tail titration) of 4 μM CRY1 PHR with BMAL1 TAD probe is denoted by a dashed cyan line, and the mean FP signal of isolated BMAL1 TAD probe is denoted by a dotted cyan line. Data represent mean ± SD from one representative assay (of $n = 3$). (*C*) Competition assay in which CRY1 tail (black), exon 11 (gray), or the Δ11 tail (magenta) is titrated into a mixture of 4 μM CRY1 PHR and 20 nM fluorescently labeled CLOCK PAS-B probe. Mean FP signal ($n = 14$ points from same plate as titration) of 4 μM CRY1 PHR CLOCK PAS-B probe is denoted by a dashed green line, and the mean FP signal of isolated CLOCK PAS-B probe is denoted by a dotted green line. Data represent mean ± SD from one representative assay (of $n = 3$). Curves represent fit to one-site competitive binding model (Prism). (*D* and *E*) BLI sensorgram for biotinylated CLOCK:BMAL1 PAS-AB titrated with full-length CRY1 (*E*, gray to black) or CRY1Δ11 (pink to magenta). Model fit to association and dissociation over time represented by thin blue line. (*F–H*) Fits for K_D, k_{on}, and k_{off} from kinetic analysis of BLI data. $^*P < 0.05$; $^{**}P < 0.01$ determined by one-way unpaired ANOVA and Tukey's multiple-comparison test. Nonsignificant differences ($P > 0.05$) is denoted by "ns." (*I*) Steady-state analysis of BLI response versus CRY1 full-length (black) or CRY1Δ11 (magenta) concentration (from data in *D* and *E*, respectively). Plot shows the mean representative binding curves of samples (of $n = 3$ independent assays). Curve represents fit to one-site binding (Prism). (*J*) Fits for K_D from steady-state analysis of BLI data. $^*P < 0.05$; $^{**}P < 0.01$ determined by one-way unpaired ANOVA and Tukey's multiple-comparison test. Nonsignificant differences ($P > 0.05$) are denoted by "ns." (*K*) *Per1-Luc* assay in HEK293T cells with plasmids encoding human *Cry1* WT-Flag-Myc-His (black) or *Cry1* Δ11-Flag-Myc-His (magenta) with mouse *Clock* WT (C) or W362A, and mouse *Bmal1* WT (B), L606A L607A (LL/AA) or 619X. Relative activity is normalized to each *Clock-Bmal1* construct (set to 1) in the absence of *Cry1*. Error bars, SD of 11 measurements across three assay repeats; $^{****}P < 0.0001$ compared by two-tailed *t* test. (*L*) Western blots showing expression of transiently transfected CRY protein (α-Myc) or a histone H3 loading control.

PER2 CBD into a preformed complex of the CRY1 PHR with its fluorescently labeled tail to show that the PER2 CBD efficiently displaced the CRY1 tail from the CRY1 PHR domain (Fig. 4*D*). Therefore, binding of the PER2 CBD and the CRY1 tail to the PHR domain appear to be mutually exclusive. This suggests that regulation of CRY1 function in the clock by exon 11 is most

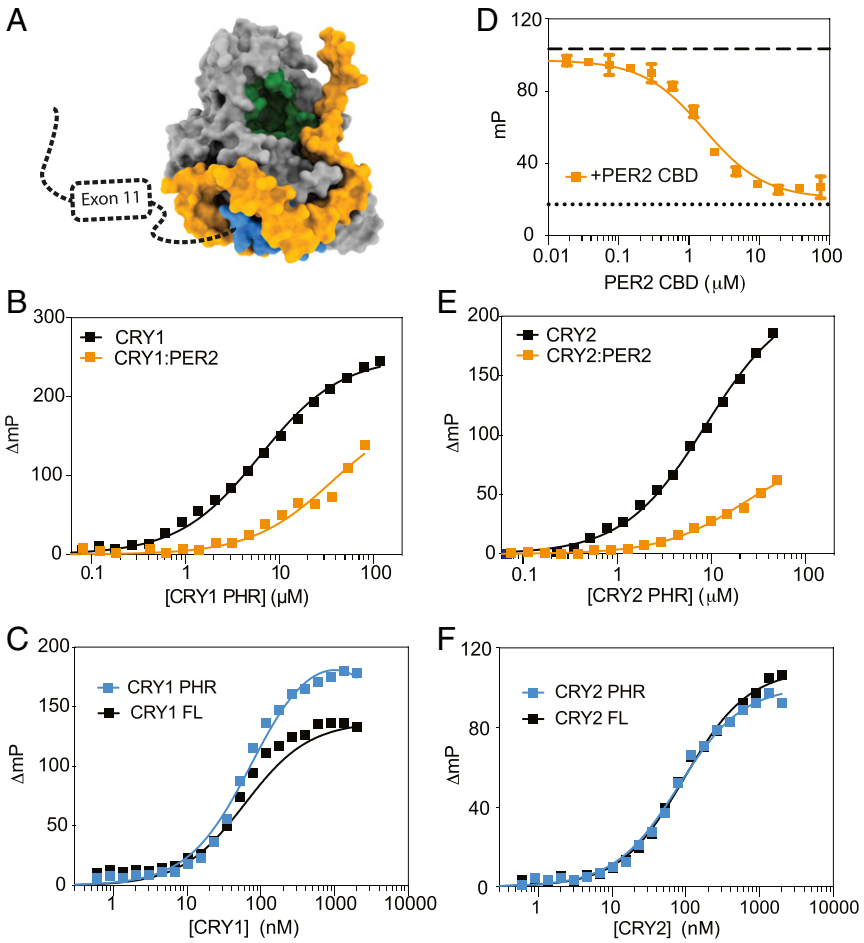

Fig. 4. PER2 competes with the CRY1 tail for binding to the PHR domain. (*A*) Crystal structure of the CRY1 PHR:PER2 CBD complex (PDB: 4CT0) illustrating the proximity of PER2 CBD (PER2 1095 to 1215; orange) to the CLOCK (green) and BMAL1 (blue) binding sites on the CRY1 PHR (gray). (*B*) FP binding curves of fluorescently labeled human tail to the CRY1 PHR (black) or a CRY1 PHR:PER2 CBD complex (orange). Plot shows the mean representative binding curves of duplicate samples ± SD (of $n = 3$ independent assays). Curve represents fit to one-site binding (Prism). (*C*) FP binding curves of fluorescently labeled PER2 CBD to the CRY1 PHR (cyan) or full-length CRY1 (black). Plot shows the mean representative binding curves of duplicate samples ± SD (of $n = 3$ independent assays). Curve represents fit to one-site binding (Prism) with PER2 CBD binding to the CRY1 PHR at $K_D = 64.8 \pm 24.9$ nM and PER2 CBD binding to CRY1 FL at $K_D = 75.3 \pm 3.7$ nM. (*D*) FP-based equilibrium competition assay in which PER2 CBD (orange) is titrated into a mixture of 4 μM CRY1 PHR and 20 nM fluorescently labeled CRY1 tail probe. Mean FP signal ($n = 13$ points from same plate as PER2 CBD titration) of 4 μM CRY1 PHR and 20 nM CRY1 tail probe is denoted by a dashed black line, and the mean FP signal of isolated CRY1 tail probe is denoted by a dotted black line. Data represent mean ± SD from one representative assay (of $n = 3$). For assays with displacement, curves represent fit to one-site competitive binding model (Prism). (*E*) FP binding curves of fluorescently labeled human tail to the CRY2 PHR (black) or a CRY2 PHR:PER2 CBD complex (orange). Plot shows the mean representative binding curves of duplicate samples ± SD (of $n = 3$ independent assays). Curve represents fit to one-site binding (Prism). (*F*) FP binding curves of fluorescently labeled PER2 CBD to the CRY2 PHR (cyan) or full-length CRY2 (black). Plot shows the mean representative binding curves of duplicate samples ± SD (of $n = 3$ independent assays). Curve represents fit to one-site binding (Prism), with PER2 CBD binding to the CRY2 PHR at $K_D = 70.5 \pm 7.8$ nM and PER2 CBD binding to CRY2 FL at $K_D = 99.8 \pm 15$ nM.

likely to occur in the late repressive complex at CT0 to CT4 when CRY1 represses CLOCK:BMAL1 independently of PER proteins (24, 38).

PHR–Tail Interactions Are Conserved in CRY2. Unlike CRY1, circadian repressive complexes that contain CRY2 obligately contain PER proteins (38). Although the CRY1 and CRY2 tails are highly divergent in sequence, their PHR domains are highly conserved with 80% identity (*SI Appendix*, Fig. S4). Therefore, we sought to determine how the PHR–tail interactions identified earlier in CRY2 (26) compare in affinity to CRY1 and if they too are affected by PER binding. We performed an FP binding assay with fluorescently labeled CRY2 tail and PHR domain to find that the CRY2 tail binds to its PHR with an affinity similar to that of CRY1 (CRY2 tail $K_D = 7.53 \pm 3.49$ μM; CRY1 tail $K_D = 4.81 \pm 0.95$ μM) (Fig. 4*E*). Interestingly, we found that the fluorescently labeled CRY1 tail also bound to the CRY2 PHR domain with similar affinity (*SI Appendix*, Fig. S4*C*), suggesting that tail binding site(s) on the PHR domains may be conserved between the two paralogs. Furthermore, we found that the PER2 CBD similarly reduced affinity of the CRY2 tail for its PHR domain (Fig. 4*E*) and that inclusion of the tail in full-length CRY2 had no effect on PER2 CBD binding (Fig. 4*F*). Altogether, these data demonstrate that PHR–tail interactions are a conserved biochemical property of mammalian cryptochromes and that PER2 binding competes with the disordered tails of both CRY1 and CRY2 for binding to the PHR domain.

Discussion

The human *Cry1Δ11* allele lengthens circadian period and consequently delays the release of melatonin and onset of sleep associated with DSPD. Mechanistically, the change in circadian

period is likely due to enhanced repression by the CRY1Δ11 mutant that was reported in cellular studies (14). We demonstrate here that exon 11 is necessary and sufficient to regulate CRY1 affinity for the PAS domain core of CLOCK:BMAL1, leading to an increase in repression. Although the change in K_D for CLOCK:BMAL1 upon deletion of exon 11 is relatively modest (approximately fourfold), this is similar to what has been observed in other proteins upon removal of analogous autoinhibitory domains (44, 45). Moreover, we previously showed that tuning CRY1 affinity for the BMAL1 TAD over a similar range of K_D values elicited comparable changes in period in cellular circadian rhythms (4, 5), providing compelling evidence that the change in affinity of CRY1 for CLOCK:BMAL1 measured here underlies physiologically relevant effects on human circadian rhythms.

Our discovery that the disordered tail of CRY1 binds directly to its PHR domain provides a framework to begin to understand how truncations, substitutions, and posttranslational modifications of the CRY1 tail influence circadian period (15–20). While exon 11 controls affinity for CLOCK:BMAL1, our NMR studies also identified a PHR-binding epitope upstream in exon 10, consistent with our exon-based truncation studies showing that exons 10 to 11 comprise the core PHR-binding motif. Although the DNA damage-dependent phosphorylation of S588 (pS588) or a phosphomimetic mutation (S588D) downstream in exon 12 both regulate proteasomal degradation of CRY1 (18–20), we saw no effect of the phosphomimetic mutant on affinity of the tail for the PHR domain. The stabilizing effect of pS588 or S588D may be related to an interaction between the CRY1 tail and the herpes virus-associated ubiquitin-specific protease (HAUSP, also known as USP7), which promotes deubiquitination of CRY1 (20). Identifying how the tail binds to regulatory proteins like HAUSP and where it docks on the PHR domain will provide key insight into its regulation of CRY1 stability and circadian rhythms.

Although both cryptochromes serve as transcriptional repressors of CLOCK:BMAL1, genetic deletion of CRY1 or CRY2 in mice leads to dramatically different circadian periods. Loss of the stronger repressor, CRY1, leads to a short period, while loss of the weaker repressor, CRY2, gives rise to a long period (46, 47). Consistent with this, the intracellular ratio of cryptochromes can define the repressive potential of the negative arm of the molecular clock to contribute to period generation (16). Remarkably, differences in their repressive power of cryptochrome isoforms is defined by biochemical differences in the secondary pocket on their PHR domains and their respective C-terminal tails; swapping several pocket residues and the tails is sufficient to confer CRY2-like repression and clock timing to CRY1 and vice versa (17). Isoform-specific differences in protein dynamics at the secondary pocket contribute to a 20-fold difference in affinity for the PAS domain core of CLOCK:BMAL1 between CRY1 and CRY2 (3). However, it was not clear until now how the disordered tails of cryptochromes might figure into regulation of CRY function in the molecular clock. This work demonstrates how PHR–tail interactions in CRY1 converge on regulation of CLOCK:BMAL1 binding at the secondary pocket of CRY1. PHR–tail interactions likely regulate CRY2 as well, since the disordered tail of CRY2 tail also binds its PHR domain (26) and posttranslational modifications in the tail regulate CRY2 stability (48). Collectively, these data demonstrate that there is much more to learn about these cryptic regulatory domains and how they influence circadian rhythms.

This work reveals a general mechanism for CRY regulation that is apparently conserved from human CRY1 to cryptochromes from *Arabidopsis* and *Drosophila*, where C-terminal tails bind to their respective PHR domains to create autoinhibited states (*SI Appendix*, Fig. S5) (26, 28, 49–52). In this respect, the CRY1Δ11 mutant appears to functionally mimic *Drosophila* CRY mutants that are constitutively active due to removal of their autoinhibitory C-terminal tail (49–51). However, unlike cryptochromes from *Arabidopsis* and *Drosophila* that use blue light to regulate the PHR–tail interaction (26, 28, 49, 53), mammalian cryptochromes do not copurify with flavin (54) or respond to blue light in their roles as transcriptional repressors (55). As an alternative to regulation by phototransduction, our data suggest that the association of other proteins (56) or posttranslational modifications (18–20) likely play direct roles in regulating the CRY1 PHR–tail interaction (*SI Appendix*, Fig. S5). Use of a flexibly tethered autoinhibitory domain to tune CRY1 activity in the clock is also consistent with a growing appreciation that intrinsically disordered regions offer a powerful means to modulate protein activity via regulated alternate splicing (57).

Materials and Methods

Expression and Purification of Recombinant Proteins. All CRY1 tail constructs (full-length human CRY1 tail, residues 496 to 586; human CRY1 exon 11, residues 530 to 553; Δ11 tail, residues 496 to 586 missing residues 530 to 553; human CRY1 exons 10 to 11, residues 496 to 553; mouse CRY1 tail, residues 496 to 606) and other proteins such as PER2 CBD (human PER2 residues 1095 to 1215), CLOCK PAS-B (mouse CLOCK residues 261 to 395), and biotin acceptor peptide (BAP)-tagged CLOCK PAS-AB (mouse CLOCK residues 93 to 395) were expressed using *Escherichia coli* Rosetta2 (DE3) cells. Sortase A and BirA were expressed in BL21 (DE3) *E. coli*. Proteins were expressed as a fusion to the solubilizing tags GST (for BirA), His_6-GST (for CRY1 and PER2 constructs), His_6-NusA-XL (for CLOCK PAS-B and BAP-tagged CLOCK PAS-AB), or His_6 (for Sortase A). Protein expression was induced at 37 °C with 0.5 mM isopropyl-β-D-thiogalactopyranoside at an OD_{600} of ∼0.8 and grown for an additional 16 h at 18 °C. Cells were centrifuged at 4 °C at 3,200 × *g*, reconstituted in 50 mM Tris, pH 7.5, 300 mM NaCl, 5% (vol/vol) glycerol, and 5 mM β-mercaptoethanol (BME), and lysed using a microfluidizer followed by brief sonication. After clarifying lysate on a centrifuge at 4 °C at 140,500 × *g* for 1 h, protein was captured using Ni-NTA affinity chromatography (Qiagen) or glutathione sepharose 4B resin (GE Life Sciences). After capturing protein on the relevant affinity chromatography resin, the affinity and solubility tags (e.g., His_6-GST, His_6, or GST) were cleaved using GST-TEV (on glutathione resin) or His_6-TEV protease (on Ni-NTA resin) at 4 °C overnight. Cleaved protein was then collected from the flow-through after overnight TEV cleavage. Sortase A and CRY1 tail constructs were further purified using size exclusion chromatography (SEC) in 50 mM Tris, pH 7.5, 150 mM NaCl, and 10% (vol/vol) glycerol. GST-BirA was further purified using SEC in 50 mM Tris, pH 8.0, 300 mM NaCl, 1 mM DTT, and 5% (vol/vol) glycerol. All other proteins (e.g., CLOCK PAS-B, CLOCK PAS-AB) were further purified using SEC in 20 mM Hepes, pH 7.5, 125 mM NaCl, 5% (vol/vol) glycerol, and 2 mM Tris(2-carboxyethyl)phosphine (TCEP). For long-term storage, small aliquots of these proteins were frozen in liquid nitrogen and stored at −70 °C.

BMAL1 PAS-AB (mouse BMAL1 residues 136 to 441) and all CRY1 constructs containing the PHR domain (mouse CRY1 PHR, residues 1 to 491; full-length mouse CRY1, residues 1 to 606; full-length human CRY1, residues 1 to 586; human CRY1 Δ11, residues 1 to 586 Δ530 to 553; mouse CRY2 PHR, residues 1 to 512; full-length mouse CRY1, residues 1 to 592) were expressed in Sf9 suspension insect cells (Expression Systems) using the baculovirus expression system. His_6-tagged versions of CRYs were cloned into pFastBac HTa vectors that were later transduced into baculovirus. We used P3 virus to infect Sf9 cells at 1.2×10^6 cells per mL, which were grown for 72 h at 27 °C before harvesting.

CRY-expressing cells were centrifuged at 4 °C at 3,200 × *g*, resuspended in 50 mM Tris, pH 7.5, 300 mM NaCl, 5% (vol/vol) glycerol, and 5 mM BME and lysed in low concentrations of detergent (0.01% [vol/vol] Triton X-100), Pierce Protease Inhibitor EDTA-free tablets (1 tablet/50 mL; Thermo Scientific), and 1 mM phenylmethylsulfonyl fluoride using a microfluidizer followed by brief sonication. After clarifying lysate on a centrifuge at 4 °C at 140,500 × *g* for 1 h, protein was captured using Ni-NTA affinity chromatography (Qiagen). Protein was further purified using ion exchange chromatography preceding SEC into CRY buffer (20 mM Hepes, pH 7.5, 125 mM NaCl, 5% [vol/vol] glycerol, and 2 mM TCEP). CRY protein preps were stored on ice at 4 °C or frozen in small aliquots and subjected to only one freeze/thaw cycle. If kept on ice, full-length (or Δ11) CRY proteins were used for experiments within 36 h of purification to minimize proteolysis of the tail, while PHR domains were used within 7 d.

BMAL1 PAS-AB expressing cells were resuspended in BMAL1 resuspension buffer (50 mM Hepes buffer pH 7.5, 300 mM NaCl, 5% [vol/vol] glycerol, and 5 mM BME). Cells were lysed and clarified as described above. The soluble lysate was bound in batch mode to glutathione sepharose 4B (GE Healthcare), then washed in BMAL1 resuspension buffer and eluted with 50 mM Hepes buffer, pH 7.5, 150 mM NaCl, 5% (vol/vol) glycerol, and 5 mM BME, 25 mM reduced glutathione. The protein was desalted into 50 mM Hepes buffer, pH 7, 150 mM NaCl, 5% (vol/vol) glycerol, and 5 mM BME using a HiTrap Desalting column (GE Healthcare), and the GST tag was cleaved with GST-TEV protease overnight at 4 °C. The cleaved GST-tag and GST-tagged TEV protease was removed by glutathione sepharose 4B (GE Healthcare), and the remaining BMAL1 PAS-AB protein was further purified by Superdex75 SEC (GE Healthcare) into 20 mM Hepes buffer, pH 7.5, 125 mM NaCl, 5% (vol/vol) glycerol, and 2 mM TCEP. Purified BMAL1 PAS-AB was mixed with biotinylated CLOCK PAS-AB (below) to generate the heterodimer for binding assays.

Biotinylation and Reconstitution of CLOCK:BMAL1 PAS-AB. For the biotinylation reaction, 100 μM BAP-CLOCK PAS-AB in 20 mM Hepes, pH 7.5, 125 mM NaCl, 5% (vol/vol) glycerol, and 2 mM TCEP was incubated at 4 °C overnight with 2 mM ATP, 1 μM GST-BirA, and 150 μM biotin. GST-BirA was removed after the reaction using glutathione sepharose 4B (GE Healthcare) resin, and excess biotin was separated from the labeled protein by SEC. Biotin-CLOCK:BMAL1 PAS-AB heterodimer was reconstituted after labeling by adding equimolar BMAL1 PAS-AB to biotinylated CLOCK PAS-AB and verifying complex formation by SEC. Biotinylated heterodimer was quick frozen in liquid nitrogen for long-term storage at −80 °C.

Fluorescent Labeling of Peptides and Proteins. For shorter peptides such as CRY1 exon 11, BMAL1 TAD, and the Sortase A recognition motif, we purchased commercially synthesized peptides with N-terminal cysteines conjugated to tetramethylrhodamine (TAMRA) 5-maleimide fluorophore or a fluorescein 5-maleimide fluorophore. To fluorescently label recombinantly expressed proteins and peptides, we utilized Sortase A-mediated reactions (58) between an N-terminally fluorescein-labeled (or TAMRA-labeled) Sortase A recognition motif peptide (FAM-LPETGG) and our protein of interest (e.g., CRY1 tail or CLOCK PAS-B). CLOCK PAS-B were labeled right after purification via SEC (i.e., without a freeze/thaw cycle). Reactions were carried out in 50 mM Tris, pH 7.5, 150 mM NaCl, and 10 mM $CaCl_2$ using 5 μM His_6-Sortase A and 3 to 5× molar excess of the fluorescently labeled Sortase A recognition motif peptide relative to the protein to be labeled. Labeled protein was purified from the reaction mixture using Ni-NTA affinity chromatography (Qiagen) and/or followed by SEC. Labeled protein was characterized by fluorescent imaging on an SDS/PAGE gel using a Typhoon imager (GE Healthcare). Extent of labeling was measured through spectrophotometry and calculated using the following equation:

$$\%_{\text{labeled}} = \frac{A_{\text{dye}}}{\varepsilon_{\text{dye}} \times \left(\frac{A_{280} - (A_{\text{dye}} \times \text{CF})}{\varepsilon_{\text{protein}}}\right)},$$

where A_{dye} is the absorbance at the maximum absorption wavelength (555 nm for TAMRA and 494 nm for fluorescein), ε_{dye} is the extinction coefficient of the dye (65,000 $M^{-1}{\cdot}cm^{-1}$ for TAMRA and 68,000 $M^{-1}{\cdot}cm^{-1}$ for fluorescein), and CF is a correction factor that adjusts for the amount of absorbance at 280 nm contributed by the dye (59). We also measured molecular weights of fluorescent probe using a SciEx QTOF mass spectrometer. All probes were labeled with at least 60% efficiency.

FP. All FP assays were performed in 50 mM Bis-Tris propane, pH 7.5, 100 mM NaCl, 0.05% (vol/vol) Tween, and 2 mM TCEP. For direct binding assays, varying amounts of CRY protein was mixed with 0.02 μM of a fluorescently labeled tail construct. Reactions were incubated for 10 min at room temperature. For displacement assays, 0.02 μM fluorescently labeled probe (BMAL1 TAD, CLOCK PAS-B, or hCRY1 tail) were incubated with 4 μM CRY1 PHR for 3 h on ice. Varying amounts of unlabeled CRY tail constructs were mixed with this reaction and incubated for 10 min at room temperature. FP measurements were measured on a Perkin-Elmer EnVision 2103 Multilabel plate reader with excitation at 485 nm and emission at 535 nm. The equilibrium dissociation constant (K_D) and extent of nonspecific binding was calculated by fitting millipolarization level (mp) to a one-site total model in GraphPad Prism using averaged mp values from assays with duplicate samples. IC_{50} values were calculated from displacement assays by fitting the mp level to a one-site competitive binding model in GraphPad Prism, with averaged mp values from assays with duplicate samples. Data shown are from one representative experiment (± SD) of three independent assays.

NMR Spectroscopy. All experiments were performed on a Bruker Avance 800-MHz spectrometer equipped with cryogenic probes. Spectra shown for experiments were collected using 20 mM MES buffer, pH 6.8, 100 mM NaCl, 4 mM TCEP, 1 mM EDTA, and 10% (vol/vol) D_2O at 298 K. Spectra were processed using nmrPipe and analyzed with Sparky and CCPNMR (60–62). The backbone assignment of the human CRY1 tail was accomplished using standard NH-edited triple-resonance experiments [HN(CA)CO, HNCO, HNCACB, CBCA(CO)NH] and four-dimensional carbon detection methods such as (HACA)N(CA)CON and (HACA)N(CA)NCO (27). We were able to assign 79 nonambiguous peaks out of 97 possible residues on the CON spectra. Chemical shift perturbation (Δδ) or the change in two-dimensional CON peak position was calculated using the following equation:

$$\Delta\delta = \sqrt{\left(\text{N}\Delta_{\text{ppm}}\alpha\right)^2 + \left(\text{CO}\Delta_{\text{ppm}}\right)^2},$$

where Δ_{ppm} is the change in chemical shift and a value of $\alpha = 0.3$ was used to normalize between ^{15}N and ^{13}C chemical shift ranges (63).

Biolayer Interferometry. All BLI experiments were performed using an eight-channel Octet-RED96e (ForteBio). All BLI experiments were performed in BLI assay buffer (20 mM Hepes, pH 7.5, 125 mM NaCl, 5% [vol/vol] glycerol, 2 mM TCEP). For experiments containing full-length CRY1 or CRY1Δ11, we added 0.5 mM EDTA to the BLI buffer. For each experiment, we used eight streptavidin biosensor tips (ForteBio). All experiments began with reference measurements using unloaded streptavidin tips to establish a baseline in BLI buffer, after which nonspecific CRY1 association was measured for 5 min in wells containing twofold serial dilutions of CRY1 (e.g., 4, 2, 1, 0.5, 0.25 μM, etc.) or a reference sample well containing no CRY, and then dissociation was subsequently measured for 5 min in wells containing BLI buffer. After measuring our initial reference, we repeated the same assay with fresh tips that were loaded with 1.5 to 3 μg/mL biotinylated CLOCK:BMAL PAS-AB dimer using BLI buffer that contained no BSA or Tween 20. Data were processed and fitted using Octet software, version 7 (ForteBio). Before fitting, all datasets were reference-subtracted, aligned on the *y* axis through their respective baselines, aligned for interstep correction through their respective dissociation steps, and finally smoothened using Savitzy–Golay filtering. For each experiment, at least four different concentrations were used to fit association and dissociation globally over the full range of the experiment using a 1:1 binding model in Octet software, version 7 (ForteBio). Goodness of fit was determined with χ^2 and R^2 tests that conform to the manufacturer's guidelines.

Cellular Assays. *Per1-Luc* reporter-gene assays investigating repression by CRY1 were performed as before (4). Briefly, plasmids were transfected into HEK293T cells (ATCC) in a 48-well plate in duplicate with LT-1 transfection reagent (Mirus) at the indicated concentrations: 5 ng of pGL3 *Per1-Luc* reporter, 100 ng each of pSG5 Flag-mouse *Bmal1* and pSG5 His_6-Flag-mouse *Clock*, and 50 ng of pcDNA4B human *Cry1*-Flag-Myc-His_6 (wild-type or Δ11) with empty pcDNA4 vector used to normalize total plasmid concentrations to 800 ng/well. Cells were harvested 30 h after transfection with luciferase-compatible 1× Passive Lysis Buffer (NEB), and luciferase activity was assayed with Bright-Glo luciferin reagent (Promega) on an EnVision plate reader (Perkin-Elmer). Statistical tests were performed on aggregated data from $n = 3$ independent assays using two-sided, two-tailed Student's *t* tests.

Protein expression of human CRY1 full-length and Δ11 was assessed by Western blotting after transfection of 200 ng of either construct into HEK293T cells in a 12-well plate. Cells were harvested 48 h later, and equal volumes of cell lysate were resolved on a 7.5% SDS/PAGE and transferred to a nitrocellulose membrane. CRY protein was detected using the anti-myc (9E10) antibody (purified in-house from the [9E10] hybridoma line purchased from the Developmental Studies Hybridoma Bank, University of Iowa). Histone H3 (1G1) antibody was used as a loading control (catalog #sc-517576; Santa Cruz Biotechnology), and both were detected with a rabbit anti-mouse IgG-horseradish peroxidase conjugate (catalog #sc-358914; Santa Cruz Biotechnology) and Clarity chemiluminescence reagents (Bio-Rad) using a ChemiDoc XRS+ CCD imager (Bio-Rad). Data are representative of $n = 2$ experiments with duplicate samples.

Data Availability. The NMR chemical shift assignments for the human CRY1 tail have been deposited in the Biological Magnetic Resonance Bank database (accession no. 27988). All study data are included in the article and *SI Appendix*.

ACKNOWLEDGMENTS. We thank Scott Showalter (Penn State) and Isabella Felli (University of Florence) for pulse sequences and advice on ^{13}C-detected CON NMR experiments. This work was funded by NIH Grants R01 GM107069 and GM121507-02S1 (to C.L.P.) and funds from the NIH Office of the Director under Award S10OD018455. G.C.G.P. is supported by a HHMI Gilliam Fellowship with additional support from the University of California, Santa Cruz Graduate Division.

1. R. Zhang, N. F. Lahens, H. I. Ballance, M. E. Hughes, J. B. Hogenesch, A circadian gene expression atlas in mammals: Implications for biology and medicine. *Proc. Natl. Acad. Sci. U.S.A.* **111**, 16219–16224 (2014).
2. C. L. Partch, C. B. Green, J. S. Takahashi, Molecular architecture of the mammalian circadian clock. *Trends Cell Biol.* **24**, 90–99 (2014).
3. J. L. Fribourgh *et al*., Dynamics at the serine loop underlie differential affinity of cryptochromes for CLOCK:BMAL1 to control circadian timing. *eLife* **9**, e55275 (2020).
4. H. Xu *et al*., Cryptochrome 1 regulates the circadian clock through dynamic interactions with the BMAL1 C terminus. *Nat. Struct. Mol. Biol.* **22**, 476–484 (2015).
5. C. L. Gustafson *et al*., A slow conformational switch in the BMAL1 transactivation domain modulates circadian rhythms. *Mol. Cell* **66**, 447–457.e7 (2017).
6. S. I. Godinho *et al*., The after-hours mutant reveals a role for Fbxl3 in determining mammalian circadian period. *Science* **316**, 897–900 (2007).
7. A. Hirano *et al*., A Cryptochrome 2 mutation yields advanced sleep phase in humans. *eLife* **5**, e16695 (2016).
8. A. Hirano *et al*., FBXL21 regulates oscillation of the circadian clock through ubiquitination and stabilization of cryptochromes. *Cell* **152**, 1106–1118 (2013).
9. S. Militi *et al*., Early doors (Edo) mutant mouse reveals the importance of period 2 (PER2) PAS domain structure for circadian pacemaking. *Proc. Natl. Acad. Sci. U.S.A.* **113**, 2756–2761 (2016).
10. K. L. Toh *et al*., An hPer2 phosphorylation site mutation in familial advanced sleep phase syndrome. *Science* **291**, 1040–1043 (2001).
11. Y. Xu *et al*., Functional consequences of a CKIdelta mutation causing familial advanced sleep phase syndrome. *Nature* **434**, 640–644 (2005).
12. Y. Xu *et al*., Modeling of a human circadian mutation yields insights into clock regulation by PER2. *Cell* **128**, 59–70 (2007).
13. C. R. Jones, A. L. Huang, L. J. Ptáček, Y. H. Fu, Genetic basis of human circadian rhythm disorders. *Exp. Neurol.* **243**, 28–33 (2013).
14. A. Patke *et al*., Mutation of the human circadian clock gene CRY1 in familial delayed sleep phase disorder. *Cell* **169**, 203–215.e13 (2017).
15. S. K. Khan *et al*., Identification of a novel cryptochrome differentiating domain required for feedback repression in circadian clock function. *J. Biol. Chem.* **287**, 25917–25926 (2012).
16. Y. Li, W. Xiong, E. E. Zhang, The ratio of intracellular CRY proteins determines the clock period length. *Biochem. Biophys. Res. Commun.* **472**, 531–538 (2016).
17. C. Rosensweig *et al*., An evolutionary hotspot defines functional differences between CRYPTOCHROMES. *Nat. Commun.* **9**, 1138 (2018).
18. P. Gao *et al*., Phosphorylation of the cryptochrome 1 C-terminal tail regulates circadian period length. *J. Biol. Chem.* **288**, 35277–35286 (2013).
19. N. Liu, E. E. Zhang, Phosphorylation regulating the ratio of intracellular CRY1 protein determines the circadian period. *Front. Neurol.* **7**, 159 (2016).
20. S. J. Papp *et al*., DNA damage shifts circadian clock time via Hausp-dependent Cry1 stabilization. *eLife* **4**, e04883 (2015).
21. A. K. Michael *et al*., Formation of a repressive complex in the mammalian circadian clock is mediated by the secondary pocket of CRY1. *Proc. Natl. Acad. Sci. U.S.A.* **114**, 1560–1565 (2017).
22. A. Czarna *et al*., Quantitative analyses of cryptochrome-mBMAL1 interactions: Mechanistic insights into the transcriptional regulation of the mammalian circadian clock. *J. Biol. Chem.* **286**, 22414–22425 (2011).
23. I. Schmalen *et al*., Interaction of circadian clock proteins CRY1 and PER2 is modulated by zinc binding and disulfide bond formation. *Cell* **157**, 1203–1215 (2014).
24. Y. Y. Chiou *et al*., Mammalian Period represses and de-represses transcription by displacing CLOCK-BMAL1 from promoters in a Cryptochrome-dependent manner. *Proc. Natl. Acad. Sci. U.S.A.* **113**, E6072–E6079 (2016).
25. S. Kosol, S. Contreras-Martos, C. Cedeño, P. Tompa, Structural characterization of intrinsically disordered proteins by NMR spectroscopy. *Molecules* **18**, 10802–10828 (2013).
26. C. L. Partch, M. W. Clarkson, S. Ozgür, A. L. Lee, A. Sancar, Role of structural plasticity in signal transduction by the cryptochrome blue-light photoreceptor. *Biochemistry* **44**, 3795–3805 (2005).
27. M. Bastidas, E. B. Gibbs, D. Sahu, S. A. Showalter, A primer for carbon-detected NMR applications to intrinsically disordered proteins in solution. *Concepts Magn. Reson. Part A* **44**, 54–66 (2015).
28. A. Czarna *et al*., Structures of *Drosophila* cryptochrome and mouse cryptochrome1 provide insight into circadian function. *Cell* **153**, 1394–1405 (2013).
29. M. Fuxreiter, I. Simon, P. Friedrich, P. Tompa, Preformed structural elements feature in partner recognition by intrinsically unstructured proteins. *J. Mol. Biol.* **338**, 1015–1026 (2004).
30. R. Pancsa, M. Fuxreiter, Interactions via intrinsically disordered regions: What kind of motifs? *IUBMB Life* **64**, 513–520 (2012).
31. N. E. Hafsa, D. Arndt, D. S. Wishart, CSI 3.0: A web server for identifying secondary and super-secondary structure in proteins using NMR chemical shifts. *Nucleic Acids Res.* **43**, W370–W377 (2015).
32. T. Trudeau *et al*., Structure and intrinsic disorder in protein autoinhibition. *Structure* **21**, 332–341 (2013).
33. S. Miller *et al*., Isoform-selective regulation of mammalian cryptochromes. *Nat. Chem. Biol.* **16**, 676–685 (2020).
34. K. Kasahara, M. Shiina, J. Higo, K. Ogata, H. Nakamura, Phosphorylation of an intrinsically disordered region of Ets1 shifts a multi-modal interaction ensemble to an auto-inhibitory state. *Nucleic Acids Res.* **46**, 2243–2251 (2018).
35. S. K. Olsen *et al*., Insights into the molecular basis for fibroblast growth factor receptor autoinhibition and ligand-binding promiscuity. *Proc. Natl. Acad. Sci. U.S.A.* **101**, 935–940 (2004).
36. H.-X. Zhou, P. A. Bates, Modeling protein association mechanisms and kinetics. *Curr. Opin. Struct. Biol.* **23**, 887–893 (2013).
37. T. K. Sato *et al*., Feedback repression is required for mammalian circadian clock function. *Nat. Genet.* **38**, 312–319 (2006).
38. N. Koike *et al*., Transcriptional architecture and chromatin landscape of the core circadian clock in mammals. *Science* **338**, 349–354 (2012).
39. R. P. Aryal *et al*., Macromolecular assemblies of the mammalian circadian clock. *Mol. Cell* **67**, 770–782.e6 (2017).
40. M. Stratmann, F. Stadler, F. Tamanini, G. T. van der Horst, J. A. Ripperger, Flexible phase adjustment of circadian albumin D site-binding protein (DBP) gene expression by CRYPTOCHROME1. *Genes Dev.* **24**, 1317–1328 (2010).
41. R. Ye *et al*., Dual modes of CLOCK:BMAL1 inhibition mediated by Cryptochrome and Period proteins in the mammalian circadian clock. *Genes Dev.* **28**, 1989–1998 (2014).
42. A. C. Liu *et al*., Intercellular coupling confers robustness against mutations in the SCN circadian clock network. *Cell* **129**, 605–616 (2007).
43. S. N. Nangle *et al*., Molecular assembly of the period-cryptochrome circadian transcriptional repressor complex. *eLife* **3**, e03674 (2014).
44. M. C. Regan *et al*., Structural and dynamic studies of the transcription factor ERG reveal DNA binding is allosterically autoinhibited. *Proc. Natl. Acad. Sci. U.S.A.* **110**, 13374–13379 (2013).
45. S. L. Currie *et al*., Structured and disordered regions cooperatively mediate DNA-binding autoinhibition of ETS factors ETV1, ETV4 and ETV5. *Nucleic Acids Res.* **45**, 2223–2241 (2017).
46. G. T. van der Horst *et al*., Mammalian Cry1 and Cry2 are essential for maintenance of circadian rhythms. *Nature* **398**, 627–630 (1999).
47. M. H. Vitaterna *et al*., Differential regulation of mammalian period genes and circadian rhythmicity by cryptochromes 1 and 2. *Proc. Natl. Acad. Sci. U.S.A.* **96**, 12114–12119 (1999).
48. N. Kurabayashi, T. Hirota, M. Sakai, K. Sanada, Y. Fukada, DYRK1A and glycogen synthase kinase 3beta, a dual-kinase mechanism directing proteasomal degradation of CRY2 for circadian timekeeping. *Mol. Cell. Biol.* **30**, 1757–1768 (2010).
49. A. Busza, M. Emery-Le, M. Rosbash, P. Emery, Roles of the two *Drosophila* CRYPTOCHROME structural domains in circadian photoreception. *Science* **304**, 1503–1506 (2004).
50. S. Dissel *et al*., A constitutively active cryptochrome in *Drosophila melanogaster*. *Nat. Neurosci.* **7**, 834–840 (2004).
51. E. Rosato *et al*., Light-dependent interaction between *Drosophila* CRY and the clock protein PER mediated by the carboxy terminus of CRY. *Curr. Biol.* **11**, 909–917 (2001).
52. B. D. Zoltowski *et al*., Structure of full-length *Drosophila* cryptochrome. *Nature* **480**, 396–399 (2011).
53. C. Levy *et al*., Updated structure of *Drosophila* cryptochrome. *Nature* **495**, E3–E4 (2013).
54. W. Xing *et al*., SCF(FBXL3) ubiquitin ligase targets cryptochromes at their cofactor pocket. *Nature* **496**, 64–68 (2013).
55. E. A. Griffin Jr, D. Staknis, C. J. Weitz, Light-independent role of CRY1 and CRY2 in the mammalian circadian clock. *Science* **286**, 768–771 (1999).
56. S. Cal-Kayitmazbatir *et al*., CRY1-CBS binding regulates circadian clock function and metabolism. *FEBS J.*, 10.1111/febs.15360 (2020).
57. M. Buljan *et al*., Alternative splicing of intrinsically disordered regions and rewiring of protein interactions. *Curr. Opin. Struct. Biol.* **23**, 443–450 (2013).
58. C. S. Theile *et al*., Site-specific N-terminal labeling of proteins using sortase-mediated reactions. *Nat. Protoc.* **8**, 1800–1807 (2013).
59. Anonymous, Calculate dye:protein (F/P) molar ratios (Tech Tip #31; TR0031.7; Thermo Scientific, 2011). http://tools.thermofisher.com/content/sfs/brochures/TR0031-Calc-FP-ratios.pdf. Accessed 30 July 2019.
60. F. Delaglio *et al*., NMRPipe: A multidimensional spectral processing system based on UNIX pipes. *J. Biomol. NMR* **6**, 277–293 (1995).
61. T. D. Goddard, D. G. Kneller, SPARKY 3 (University of California, San Francisco, 2017).
62. W. F. Vranken *et al*., The CCPN data model for NMR spectroscopy: Development of a software pipeline. *Proteins* **59**, 687–696 (2005).
63. C. W. Lawrence, A. Bonny, S. A. Showalter, The disordered C-terminus of the RNA polymerase II phosphatase FCP1 is partially helical in the unbound state. *Biochem. Biophys. Res. Commun.* **410**, 461–465 (2011).